

Multimode Strong Coupling in Superconducting Cavity Piezo-electromechanics

Xu Han, Chang-Ling Zou, and Hong X. Tang*

Department of Electrical Engineering, Yale University, New Haven, Connecticut 06511, USA

High frequency mechanical resonators subjected to low thermal phonon occupancy are easier to be prepared to the ground state by direct cryogenic cooling. Their extreme stiffness, however, poses a significant challenge for external interrogations. Here we demonstrate a superconducting cavity piezo-electromechanical system in which multiple modes of a bulk acoustic resonator oscillating at 10 GHz are coupled to a planar microwave superconducting resonator with a cooperativity exceeding 2×10^3 , deep in the strong coupling regime. By implementation of the non-contact coupling scheme to reduce mechanical dissipation, the system exhibits excellent coherence characterized by a frequency-quality factor product of 7.5×10^{15} Hz. Interesting dynamics of temporal oscillations of the microwave energy is observed, implying the coherent conversion between phonons and photons. The demonstrated high frequency cavity piezo-electromechanics is compatible with superconducting qubits, representing an important step towards hybrid quantum systems.

Introduction.- Controlling mechanical motion by electromagnetic field has recently emerged as a new field of great interest [1–3]. Impressive progresses have been achieved in various cavity electro/optomechanical systems, including ground-state cooling of mechanical resonators [4–6], quantum squeezing of a mechanical mode [7, 8], and efficient conversion between photons at vastly different frequencies [9–11]. To realize coherent quantum operations, the mechanical resonator needs to be prepared in the ground state and the photon-phonon coupling rate must overcome the energy dissipation rate of each individual system to its local environment, reaching the so-called strong coupling regime [12–15]. For this reason, realizing strong coupling in a high frequency mechanical system is desirable since higher mechanical resonant frequency (ω_m) translates to lower thermal phonon occupation number ($\bar{n} \approx k_B T / \hbar \omega_m$, where k_B is Boltzmann’s constant and T is the temperature) and hence eases refrigeration conditions for reaching the ground state ($\bar{n} \ll 1$). Particularly, mechanical resonators above ~ 10 GHz can be cooled to ground state by direct dilution refrigeration without the necessity of active cooling techniques such as feedback cooling [16, 17] and sideband cooling [4, 5, 18].

In this perspective, great efforts have been dedicated to realizing coherent cavity electro/optomechanical coupling in high frequency regime [19–25]. One remarkable breakthrough in experiment has been achieved by Cleland group [20], who demonstrated the ground state cooling of a 6-GHz piezoelectric bulk acoustic resonator (BAR) and the interrogation of its quantum states with a superconducting phase qubit. However, the potential of this important class of high frequency mechanical systems can only be fully explored if its quality factor (Q factor) is further improved; even though the intrinsic Q factor of the mechanical resonator in principle can exceed 10^5 , the demonstrated Q is only 260 and the phonon lifetime is limited to 6 ns in Ref. [20]. Furthermore, the wavelength of phonon at 10 GHz is more than four orders of magnitude smaller than that of microwave pho-

ton. This allows not only the reduction of the device footprint but also the study of multimode physics beyond the single mode limitation in usual microwave resonators, where a wealth of new phenomena emerges [26–30].

In this Letter, we demonstrate a high- Q superconducting cavity electromechanical system operating at 10 GHz in which a planar superconducting microwave resonator is placed over an aluminum nitride-on-silicon (AlN-on-Si) BAR in a non-contact configuration. By harnessing the strong piezoelectric effect of AlN [22, 23, 31], we are able to strongly couple the microwave mode with an array of acoustic thickness modes of the BAR simultaneously. Due to the non-contact-electrode coupling scheme, our system exhibits a high mechanical quality factor of 7.5×10^5 and a high frequency-quality factor product ($f \cdot Q$) of 7.5×10^{15} Hz at 1.7 K, improving the phonon lifetime to 11 μ s at 10 GHz. Benchmark phenomena of a strongly coupled system including avoided crossing spectra and coherent temporal oscillations are observed, featuring a high cooperativity of $C \approx 2178$. Although our experiments are conducted at 1.7 K, further refrigeration to millikelvins would bring this high-performance multimode system to the quantum regime, providing a new route for studying the complex quantum dynamics such as entanglement between mechanical modes [32, 33].

Cavity Piezo-electromechanical Coupling.- The piezoelectric interaction can be characterized by the extra electric energy due to the strain induced polarization $H_{piezo} = \int (\Delta \mathbf{P} \cdot \mathbf{E}) dV = \int [(\mathbf{e} \cdot \mathbf{S}) \cdot \mathbf{E}] dV$, where \mathbf{P} and \mathbf{E} are the electric polarization and the electric field vectors in the material, respectively, \mathbf{S} is the second-rank strain tensor, \mathbf{e} is the third-rank piezoelectric coefficient tensor of the material. In contrast to other electromechanical coupling mechanisms, such as capacitive coupling and electrostriction where the interaction depends on $|\mathbf{E}|^2$, the piezoelectric effect provides direct linear coupling between the electrical field and the mechanical motion, which in the following we refer as “piezo-electromechanical” coupling.

To illustrate the concept of cavity piezo-

electromechanical coupling, we consider a piezoelectric film BAR sandwiched between the parallel capacitor plates of an “inductor-capacitor” (LC) resonator [Fig. 1(a)]. Thickness modes of the BAR form standing longitudinal acoustic waves with the mechanical displacement sinusoidally distributed in z -direction [orange lines in Fig. 1(a)]. Due to the piezoelectric effect, the oscillating voltage on the capacitor will compress and expand the film, thus actuating the mechanical motion; conversely, the strain in the film will induce excess electric polarization in the dielectric, hence producing oscillating voltage and current in the LC resonator. It should be noted that the coupling between the LC resonator and the piezoelectric BAR do not require electrodes to directly contact with the BAR. In fact, contactless coupling is preferred because contacting metals and metal-dielectric interfaces are known to cause mechanical dissipation [34]. The non-contact excitation mechanism has also been recently explored in air-gap piezoelectric MEMS devices [35]. The elimination of metal from piezoelectric structures also allows the construction of high- Q optomechanical resonators without metal induced light absorption, making it possible to simultaneously couple acoustic modes to both microwave and optical photons for realizing microwave-to-optical conversions [3, 21].

The linear piezo-electromechanical system can be described by a Hamiltonian of coupled modes under the rotating-wave approximation as

$$H/\hbar = \omega_a a^\dagger a + \sum_n \omega_{bn} b_n^\dagger b_n + \sum_n g_n (a^\dagger b_n + a b_n^\dagger), \quad (1)$$

where a (a^\dagger) and b_n (b_n^\dagger) are the annihilation (creation) operators for microwave photons at frequency ω_a and phonons of the n -th order mechanical mode at frequency ω_{bn} , respectively, and g_n is the coupling strength between them. In this work, we focus on acoustic thickness modes with the zz -component strain (S_{zz}) piezoelectrically coupled to the z -component electric field (E_z). Then g_n can be expressed as [36]

$$g_n = \frac{e_{33}}{2\sqrt{\epsilon_0\rho}} \sqrt{\frac{\omega_a}{\omega_{bn}}} \int_{V_{piezo}} \zeta_z(\mathbf{r}) \frac{\partial}{\partial z} \xi_{nz}(\mathbf{r}) dV, \quad (2)$$

where e_{33} is the 33-component of the piezoelectric coefficient under the contracted Voigt notation, ϵ_0 is the vacuum permittivity, and ρ is the mass density of the mechanical resonator. ζ_z and ξ_{nz} are the z -components of the normalized electric mode profile $\boldsymbol{\zeta}(\mathbf{r})$ and the mechanical displacement mode profile $\boldsymbol{\xi}(\mathbf{r})$ satisfying $\int \epsilon_r(\mathbf{r}) |\boldsymbol{\zeta}(\mathbf{r})|^2 dV = 1$ and $\int |\boldsymbol{\xi}_n(\mathbf{r})|^2 dV = 1$, respectively, with ϵ_r being the relative dielectric constant. The integral takes place within the volume of the piezoelectric material V_{piezo} . By carefully engineering the cavity and the BAR structures to optimize the piezoelectric mode overlap, strong electromechanical coupling between the

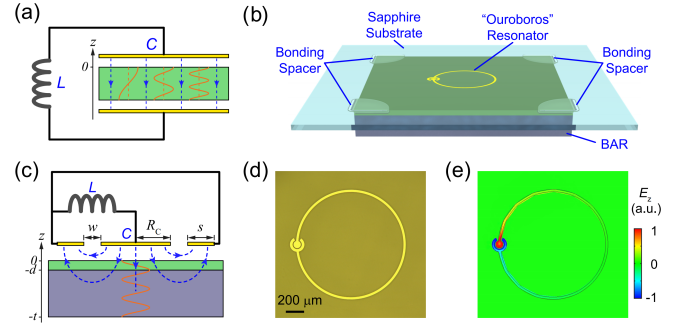


FIG. 1. (a) An illustrative configuration of a cavity piezo-electromechanical system where a piezoelectric BAR (green) is sandwiched between the parallel capacitor plates (yellow) of an LC resonator. Blue dashed lines: the electric field lines. Orange lines: amplitude distributions of the z -component mechanical displacement of different orders of acoustic thickness modes (only the first three orders of modes are drawn). (b) A schematic of the piezo-electromechanical device. (Not to scale). The planar superconducting LC resonator (“Ouroboros”) is fabricated in a 50-nm-thick niobium titanium nitride film on a 127- μm -thick sapphire substrate. The sapphire chip is flipped over and suspended on top of the BAR by the bonding spacers at the four corners of the chip. The BAR consists of a thin aluminum nitride layer (green) deposited on top of a thick oxidized high-resistivity silicon substrate. (c) A cross-sectional view of the device with the “inductor” of the “Ouroboros” indicated as an equivalent circuit. The device parameters are as following: $R_C = 40 \mu\text{m}$, $s = 30 \mu\text{m}$, $w = 10 \mu\text{m}$, $d = 550 \text{ nm}$, $t = 500 \mu\text{m}$. (d) An optical micrograph of the “Ouroboros” resonator. The long arc-shape “inductor” wire has a width of $25 \mu\text{m}$ and an average bending radius of $593 \mu\text{m}$. (e) Simulated mode profile of perpendicular electric field (E_z) of the “Ouroboros”.

microwave mode and acoustic thickness modes is feasible [36, 37].

Device Design.- Since the free spectral range (FSR) of the thickness modes is inversely proportional to the thickness of the BAR, we utilize a thick BAR to reduce the FSR so that multiple acoustic modes can be accessed simultaneously. The BAR consists of a thin piezoelectric layer of c -axis-oriented AlN deposited on top of a thick oxidized high-resistivity Si substrate, which determines an FSR $\approx \frac{v_{Si}}{2t} \approx 9.2 \text{ MHz}$, where $v_{Si} = 9.2 \text{ km/s}$ is the longitudinal acoustic wave velocity in Si and $t = 500 \mu\text{m}$ is the thickness of Si. The maximum coupling strength can be achieved when the thickness of the piezoelectric layer matches half acoustic wavelength [36]. We therefore choose the thickness of the AlN layer to be $d = 550 \text{ nm}$ to optimize the coupling strength at $\frac{\omega_{bn}}{2\pi} \approx 10 \text{ GHz}$ [23], corresponding to mode order number $n \approx 1100$. Compared with a thin-film BAR made of pure AlN, the penalty of using the high-order modes of the thick BAR is the reduction of the coupling strength by a factor of $1/\sqrt{n}$. It should be noted that even the whole BAR is made by AlN, the $1/\sqrt{n}$ scaling remains since for high-order

modes the contributions of strains with different signs in the integral in Eq. (2) cancel each other when microwave field doesn't vary much across the thickness of the BAR.

To optimize the electromechanical coupling strength, the electric field of the microwave mode should be confined around the piezoelectric layer with its lateral mode distribution matching that of the acoustic mode. Therefore, we design a planar superconducting LC resonator so that the AlN layer of the BAR can approach close proximity of the capacitor surface where the electric field is concentrated. A schematic of our device is shown in Fig. 1(b). The superconducting resonator is fabricated from a 50-nm-thick niobium titanium nitride (NbTiN) film (critical temperature $T_c \approx 13$ K) deposited on a 127- μm -thick sapphire substrate. The sapphire chip is then flipped over and suspended on top of the BAR using thin bonding spacers located at the four corners of the BAR. A tiny gap of a few microns is maintained between the sapphire and the AlN surfaces to minimize mechanical contact loss. Since the shape of our superconducting resonator resembles the ancient Greek symbol of a serpent eating its own tail, hereafter we name it as the ‘‘Ouroboros’’.

An optical micrograph of the ‘‘Ouroboros’’ resonator is shown in Fig. 1(d). The structure is patterned using e-beam lithography with hydrogen silsesquioxane (HSQ) resist followed by chlorine-based dry etching. The ‘‘Ouroboros’’ consists of a ‘‘capacitor’’ formed by a central circular pad and a surrounding ‘‘open-ring’’ pad, which are shunted by an ‘‘inductor’’ made of a long arc-shape narrow wire. The parameters of the ‘‘Ouroboros’’ [labeled in Fig. 1(c)] are designed using a finite element high frequency simulation software (HFSS) to determine the microwave resonance to be $\frac{\omega_a}{2\pi} = 10$ GHz in presence of the dielectric loading of the BAR. When the ‘‘Ouroboros’’ is excited on resonance, electric field (E_z) is concentrated and tightly confined near the capacitor pad surfaces [Fig. 1(e)], improving the mode overlap in z -direction between the microwave mode and the AlN layer. Moreover, due to the ‘‘ $\delta v/v$ ’’ effect [38], the proximal capacitor modifies the acoustic wave velocity in the BAR and creates an effective potential well in the lateral direction just under the location of capacitor, providing lateral confinement for the acoustic thickness modes. Detailed discussion on the ‘‘ $\delta v/v$ ’’ effect induced acoustic mode bounding is beyond the scope of this article and will be presented elsewhere [39]. It is worth mentioning that another advantage of the ‘‘Ouroboros’’ design is that the long-arc inductor allows supercurrents to generate magnetic flux far-extended from the chip surface, making it feasible to inductively couple the ‘‘Ouroboros’’ with an off-chip loop probe for microwave signal input and read-out. In this way, the external microwave coupling rate of the system can be easily tuned and optimized by changing the probe position and orientation.

Strong Coupling.— In order to experimentally inves-

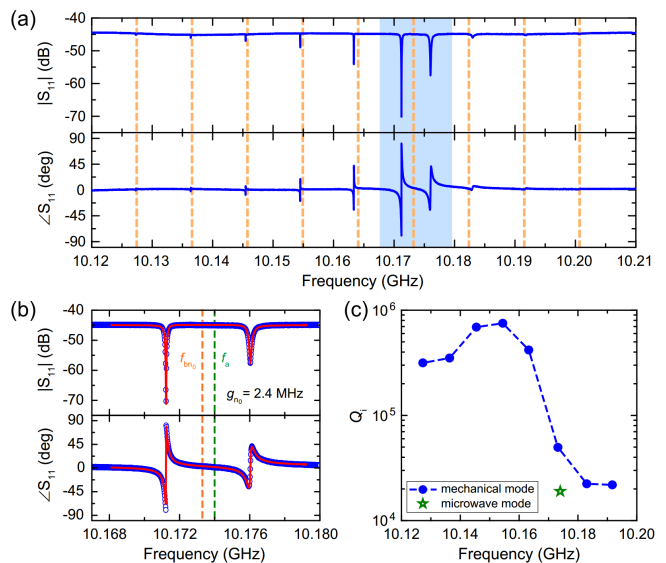


FIG. 2. (a) Microwave reflection spectrum of the device measured at 1.7 K. Orange dashed lines: unperturbed frequencies of the acoustic thickness modes of the BAR. (b) Close-up spectrum of the regime where the microwave mode strongly hybridizes with the acoustic thickness modes. Red lines: fittings using the coupled-mode formula. Green and orange dashed lines: fitted center resonant frequencies of the uncoupled microwave mode $f_a = \frac{\omega_a}{2\pi}$ and the thickness mode $f_{bn_0} = \frac{\omega_{bn_0}}{2\pi}$, respectively. (c) Fitted intrinsic quality factors of the microwave mode and the different orders of acoustic thickness modes of the BAR.

tigate the coherent cavity piezo-electromechanical coupling, the device is encapsulated in a high-conductivity copper box and loaded in a close-loop refrigerator with a base temperature of 1.62 K [40]. In all experiments, the power of the microwave probe signal is set to be below -60 dBm to avoid undesired nonlinear and heating effects in the superconducting resonator.

We first study the properties of the coupled system by probing the microwave reflection spectrum using a vector network analyzer. Figure 2(a) shows the amplitude and the phase spectra of the reflection coefficient S_{11} at 1.7 K. Several sharp resonance dips with distinct phase changes are clearly observed. Among all the resonances, the two most prominent dips at 10.171 GHz and 10.176 GHz are particularly close to each other [light blue area in Fig. 2(a)]. As the resonances become further away from these two center resonances, the mode spacing becomes more uniform and gradually approaches a constant of 9.1 MHz, which matches well with the calculated FSR of the acoustic thickness modes of the BAR. This implies that those ‘‘side bands’’ originate from thickness modes of different orders, whereas the ‘‘Ouroboros’’ resonance is mostly hybridized with a closely matched thickness mode ($n = n_0$) to produce the two hybrid resonances at 10.171 GHz and 10.176 GHz. To better visualize the coupling induced frequency shifts, we measure the fre-

quency difference between two far-separated resonances away from 10.173 GHz, and count the number of mechanical resonances between them. The ratio gives the FSR of the thickness modes which is found to be 9.12 MHz. Based on this measured FSR value, we overlay the unperturbed frequencies of thickness modes as vertical orange dashed lines in Fig. 2(a). It can be seen that the density of modes is mostly modified around the two resonances at 10.171 GHz and 10.176 GHz where the electromechanical coupling leads to strong hybridization of the microwave and the mechanical modes.

The spectra of the hybridized modes are fitted [Fig. 2(b)] by

$$S_{11}(\omega) = -1 + \frac{2\kappa_{a,e}}{-i(\omega - \omega_a) + \kappa_{a,i} + \kappa_{a,e} - \sum_n \frac{|g_n|^2}{i(\omega - \omega_{bn}) - \kappa_{bn}}}, \quad (3)$$

which is the steady-state solution of the coupled-multimode formula. Here, $\kappa_{a,i}$ and $\kappa_{a,e}$ are the intrinsic dissipation rate and the external coupling rate of the ‘‘Ouroboros’’, respectively. As expected, the fitted frequencies of the uncoupled microwave mode $\frac{\omega_a}{2\pi} = 10.1740$ GHz and the thickness mode $\frac{\omega_{bn_0}}{2\pi} = 10.1733$ GHz are very close to each other. The coupling strength is extracted to be $\frac{g_{n_0}}{2\pi} = 2.4$ MHz, larger than the dissipation rates of both the microwave mode $\frac{\kappa_{a,i} + \kappa_{a,e}}{2\pi} = 0.39$ MHz and the thickness mode $\frac{\kappa_{bn_0}}{2\pi} = 0.10$ MHz. Therefore, our system is in the strong coupling regime [14, 15] and a cooperativity of $C = g_{n_0}^2 / (\kappa_a \kappa_{bn_0}) \approx 148$ is obtained.

By this method, the intrinsic losses of all the thickness modes in the spectrum in Fig. 2(a) are extracted and the corresponding Q -factors are plotted in Fig. 2(c). A highest mechanical Q -factor of 7.5×10^5 is obtained, giving rise to an ultra-high cooperativity of $C \approx 2178$. An important figure of merit quantifying the decoupling of a mechanical resonator from the thermal environment is the $f \cdot Q$ product [41, 42]. Our system exhibits a high $f \cdot Q$ product of 7.5×10^{15} Hz at 1.7 K, more than three orders larger than previous experimental result [20]. This high $f \cdot Q$ product translates to excellent coherence characterized by a large number of coherent oscillations given by $\frac{hfQ}{k_B T} \approx 2 \times 10^5$ in presence of thermal decoherence. The asymmetry of the mechanical Q -factors with respect to the ‘‘Ouroboros’’ resonant frequency can be attributed to the microwave cavity-mediated coupling between the localized thickness modes in the potential well and the unlocalized leaky modes [39].

Temperature Dependence and Frequency Tuning.— The features of multimode strong coupling in our system are further investigated by gradually sweeping the ‘‘Ouroboros’’ resonant frequency via temperature tuning. When the temperature increases, the ‘‘Ouroboros’’ resonant frequency decreases monotonically due to the reduction of the density of Cooper pairs in the superconductor. Figure 3(a) shows the microwave reflection spectra

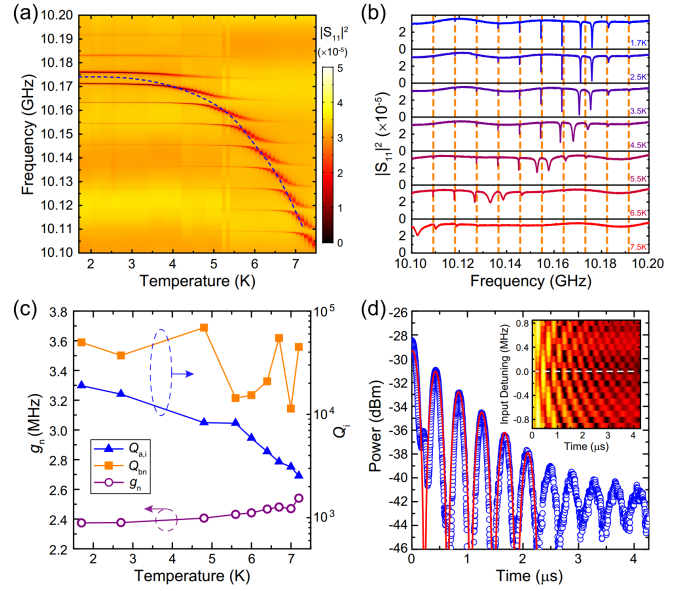


FIG. 3. (a) Temperature dependence of the microwave reflection spectra. Blue dashed line: the uncoupled ‘‘Ouroboros’’ resonant frequency obtained from the fittings using the coupled-mode formula. (b) Line plots of the microwave reflection spectra at different temperatures. Orange dashed lines: unperturbed frequencies of the acoustic thickness modes of the BAR. (c) Coupling strength and intrinsic Q -factors extracted at temperatures when the ‘‘Ouroboros’’ resonance is tuned across a thickness mode. (d) Microwave reflection in temporal domain. The center frequency of the input microwave pulse is 10.1737 GHz. Red line: the fitting of the exponentially decaying oscillation. Inset: temporal oscillations at different input frequencies detuned from 10.1737 GHz (white dashed line).

with the temperature varying from 1.7 K to 7.5 K. As the ‘‘Ouroboros’’ resonant frequency is swept over several FSRs of the thickness modes, avoided crossings are observed in sequence as a signature of multimode strong coupling (MMSC) [28, 43]. In Fig. 3(b), typical spectra at different temperatures are shown in linear plot. It can be seen that at higher temperatures the coupled modes shift dramatically to lower frequencies with increased resonance linewidths and reduced dip extinctions due to increased internal dissipation.

Using the coupled-multimode model, the uncoupled ‘‘Ouroboros’’ resonant frequency at different temperatures is extracted and plotted as the blue dashed line in Fig. 3(a), which agrees with the kinetic inductance model of thin-film superconducting resonators [44]. The BAR mechanical resonant frequencies, on the other hand, shift less than 5 Hz because of the extremely small thermal expansion coefficient of silicon within the temperature range of our experiments [45]. Figure 3(c) shows the coupling strength and the intrinsic Q -factors extracted at temperatures when the ‘‘Ouroboros’’ resonance is swept across a thickness mode. In the temperature

range we studied, g_n remains almost constant around 2.4 MHz. The intrinsic Q -factor of the “Ouroboros” gradually drops due to the increasing quasi-particle dissipation, while the Q -factors of the thickness modes show a general decreasing trend but with fluctuations, which could be attributed to property variations among different orders of modes and subject of further investigations.

Dynamics.- The strong coupling permits coherent energy exchange between coupled modes. We therefore study the dynamic interaction between the microwave and the mechanical modes in time domain. Experimentally, a short microwave excitation pulse is injected into the coupled system and the reflected power is monitored at 1.7 K. Periodical oscillations in time domain are observed with their periods depending on the center frequency of the input pulse [inset of Fig. 3(d)]. The most distinct oscillation with smallest period is observed at 10.1737 GHz [white dashed line in Fig. 3(d) inset], which matches well with the average frequency between the “Ouroboros” and the closely coupled mechanical resonance. The corresponding time trace is plotted in Fig. 3(d). Because of the fast coherent energy exchange between the strongly coupled microwave and mechanical modes, the reflected power oscillates periodically with exponentially decaying amplitude. The oscillation period is fitted to be $4.1 \mu\text{s}$ [red line in Fig. 3(d)], showing excellent agreement with the measured coupling strength $2\pi/g_n = 4.2 \mu\text{s}$. The slight deviation from the exponential decay trend for oscillation signal after around $2 \mu\text{s}$ could be attributed to the coupling between the microwave mode and multiple neighboring thickness modes.

Conclusion.- We have achieved multimode electromechanical strong coupling between a superconducting microwave resonator and a piezoelectric BAR at 10 GHz with a cooperativity of exceeding 2000. Coherent interaction has been demonstrated via the observation of the avoided-crossing spectra and the temporal oscillation of microwave energy. Due to the high operating frequency, our system can be expected to incorporate with quantum superconducting circuits for studying mechanical quantum states at relaxed refrigeration temperatures. The achieved ultra-high $f \cdot Q$ product of 7.5×10^{15} Hz and large coupling strength-over-FSR ratio of $\frac{g_n}{\text{FRS}} \approx 26\%$ allow realization of mechanical multimode quantum memory devices [27] and exploration of the intriguing superstrong coupling regime [28, 30].

Acknowledgment C.L.Z. thanks Liang Jiang for helpful discussions. This work is supported by Laboratory of Physical Sciences through a grant from Army Research Office (W911NF-14-1-0563), an Air Force Office of Scientific Research (AFOSR) MURI grant (FA9550-15-1-0029) and a NSF MRSEC grant (1119826). H.X.T. acknowledges support from a Packard Fellowship in Science and Engineering. The authors thank Michael Power and Dr. Michael Rooks for assistance in device fabrication.

* hong.tang@yale.edu

- [1] M. Tsang, “Cavity quantum electro-optics,” *Phys. Rev. A* **81**, 063837 (2010).
- [2] C. A. Regal and K. W. Lehnert, “From cavity electromechanics to cavity optomechanics,” *J. Phys. Conf. Ser.* **264**, 012025 (2011).
- [3] R. W. Andrews, R. W. Peterson, T. P. Purdy, K. Cicak, R. W. Simmonds, C. a. Regal, and K. W. Lehnert, “Bidirectional and efficient conversion between microwave and optical light,” *Nat. Phys.* **10**, 321 (2014).
- [4] J. D. Teufel, T. Donner, D. Li, J. W. Harlow, M. S. Allman, K. Cicak, a. J. Sirois, J. D. Whittaker, K. W. Lehnert, and R. W. Simmonds, “Sideband cooling of micromechanical motion to the quantum ground state,” *Nature* **475**, 359 (2011).
- [5] J. Chan, T. P. M. Alegre, A. H. Safavi-Naeini, J. T. Hill, A. Krause, S. Gröblacher, M. Aspelmeyer, and O. Painter, “Laser cooling of a nanomechanical oscillator into its quantum ground state,” *Nature* **478**, 89 (2011).
- [6] R. W. Peterson, T. P. Purdy, N. S. Kampel, R. W. Andrews, P.-L. Yu, K. W. Lehnert, and C. A. Regal, “Laser Cooling of a Micromechanical Membrane to the Quantum Backaction Limit,” *Phys. Rev. Lett.* **116**, 063601 (2016).
- [7] E. E. Wollman, C. U. Lei, a. J. Weinstein, J. Suh, A. Kronwald, F. Marquardt, a. a. Clerk, and K. C. Schwab, “Quantum squeezing of motion in a mechanical resonator,” *Science* **349**, 952 (2015).
- [8] F. Lecocq, J. B. Clark, R. W. Simmonds, J. Aumentado, and J. D. Teufel, “Quantum Nondemolition Measurement of a Nonclassical State of a Massive Object,” *Phys. Rev. X* **5**, 041037 (2015).
- [9] J. T. Hill, A. H. Safavi-Naeini, J. Chan, and O. Painter, “Coherent optical wavelength conversion via cavity optomechanics,” *Nat. Commun.* **3**, 1196 (2012).
- [10] T. Bagci, A. Simonsen, S. Schmid, L. G. Villanueva, E. Zeuthen, J. Appel, J. M. Taylor, A. Sørensen, K. Usami, A. Schliesser, and E. S. Polzik, “Optical detection of radio waves through a nanomechanical transducer,” *Nature* **507**, 81 (2014).
- [11] R. W. Andrews, A. P. Reed, K. Cicak, J. D. Teufel, and K. W. Lehnert, “Quantum-enabled temporal and spectral mode conversion of microwave signals,” *Nat. Commun.* **6**, 10021 (2015).
- [12] J. D. Teufel, D. Li, M. S. Allman, K. Cicak, a. J. Sirois, J. D. Whittaker, and R. W. Simmonds, “Circuit cavity electromechanics in the strong-coupling regime,” *Nature* **471**, 204 (2011).
- [13] E. Verhagen, S. Deléglise, S. Weis, A. Schliesser, and T. J. Kippenberg, “Quantum-coherent coupling of a mechanical oscillator to an optical cavity mode,” *Nature* **482**, 63 (2012).
- [14] X. Zhang, C.-L. Zou, L. Jiang, and H. X. Tang, “Strongly Coupled Magnons and Cavity Microwave Photons,” *Phys. Rev. Lett.* **113**, 156401 (2014).
- [15] Y. Tabuchi, S. Ishino, T. Ishikawa, R. Yamazaki, K. Usami, and Y. Nakamura, “Hybridizing Ferromagnetic Magnons and Microwave Photons in the Quantum Limit,” *Phys. Rev. Lett.* **113**, 083603 (2014).
- [16] M. Poggio, C. L. Degen, H. J. Mamin, and D. Rugar, “Feedback Cooling of a Cantilever’s Fundamental Mode below 5 mK,” *Phys. Rev. Lett.* **99**, 017201 (2007).

- [17] K. H. Lee, T. G. McRae, G. I. Harris, J. Knittel, and W. P. Bowen, “Cooling and Control of a Cavity Optomechanical System,” *Phys. Rev. Lett.* **104**, 123604 (2010).
- [18] T. a. Palomaki, J. D. Teufel, R. W. Simmonds, and K. W. Lehnert, “Entangling Mechanical Motion with Microwave Fields,” *Science* **342**, 710 (2013).
- [19] C. Xiong, L. Fan, X. Sun, and H. X. Tang, “Cavity piezooptomechanics: Piezoelectrically excited, optically transduced optomechanical resonators,” *Appl. Phys. Lett.* **102**, 021110 (2013).
- [20] A. D. O’Connell, M. Hofheinz, M. Ansmann, R. C. Bialczak, M. Lenander, E. Lucero, M. Neeley, D. Sank, H. Wang, M. Weides, J. Wenner, J. M. Martinis, and a. N. Cleland, “Quantum ground state and single-phonon control of a mechanical resonator,” *Nature* **464**, 697 (2010).
- [21] J. Bochmann, A. Vainsencher, D. D. Awschalom, and A. N. Cleland, “Nanomechanical coupling between microwave and optical photons,” *Nat. Phys.* **9**, 712 (2013).
- [22] X. Han, C. Xiong, K. Y. Fong, X. Zhang, and H. X. Tang, “Triply resonant cavity electro-optomechanics at X-band,” *New J. Phys.* **16**, 063060 (2014).
- [23] X. Han, K. Y. Fong, and H. X. Tang, “A 10-GHz film-thickness-mode cavity optomechanical resonator,” *Appl. Phys. Lett.* **106**, 161108 (2015).
- [24] J. D. Cohen, S. M. Meenehan, G. S. MacCabe, S. Gröblacher, A. H. Safavi-Naeini, F. Marsili, M. D. Shaw, and O. Painter, “Phonon counting and intensity interferometry of a nanomechanical resonator,” *Nature* **520**, 522 (2015).
- [25] K. C. Balram, M. I. Davanço, J. D. Song, and K. Srinivasan, “Coherent coupling between radiofrequency, optical and acoustic waves in piezo-optomechanical circuits,” *Nat. Photonics*, **1** (2016).
- [26] D. O. Krimer, M. Liertzer, S. Rotter, and H. E. Türeci, “Route from spontaneous decay to complex multimode dynamics in cavity QED,” *Phys. Rev. A* **89**, 033820 (2014).
- [27] X. Zhang, C.-l. Zou, N. Zhu, F. Marquardt, L. Jiang, and H. X. Tang, “Magnon dark modes and gradient memory,” *Nat. Commun.* **6**, 8914 (2015).
- [28] N. M. Sundaesan, Y. Liu, D. Sadri, L. J. Szöcs, D. L. Underwood, M. Malekakhlagh, H. E. Türeci, and A. A. Houck, “Beyond Strong Coupling in a Multimode Cavity,” *Phys. Rev. X* **5**, 021035 (2015).
- [29] N. Kostylev, M. Goryachev, and M. E. Tobar, “Superstrong coupling of a microwave cavity to yttrium iron garnet magnons,” *Appl. Phys. Lett.* **108**, 062402 (2016).
- [30] X. Zhang, C. Zou, L. Jiang, and H. X. Tang, “Superstrong coupling of thin film magnetostatic waves with microwave cavity,” *J. Appl. Phys.* **119**, 023905 (2016).
- [31] J. Stettenheim, M. Thalakulam, F. Pan, M. Bal, Z. Ji, W. Xue, L. Pfeiffer, K. W. West, M. P. Blencowe, and a. J. Rimberg, “A macroscopic mechanical resonator driven by mesoscopic electrical back-action,” *Nature* **466**, 86 (2010).
- [32] M. Schmidt, M. Ludwig, and F. Marquardt, “Optomechanical circuits for nanomechanical continuous variable quantum state processing,” *New J. Phys.* **14**, 125005 (2012).
- [33] H. Seok, L. F. Buchmann, E. M. Wright, and P. Meystre, “Multimode strong-coupling quantum optomechanics,” *Phys. Rev. A* **88**, 063850 (2013).
- [34] A. Frangi, M. Cremonesi, A. Jaakkola, and T. Pensala, “Analysis of anchor and interface losses in piezoelectric MEMS resonators,” *Sens. Actuators, A* **190**, 127 (2013).
- [35] L.-W. Hung and C. T.-C. Nguyen, “Capacitive-Piezoelectric Transducers for High-Q Micromechanical AlN Resonators,” *J. Microelectromech. Syst.* **24**, 458 (2015).
- [36] *Supplemental Material.*
- [37] C.-L. Zou, X. Han, L. Jiang, and H. X. Tang, “Cavity piezomechanical strong coupling and frequency conversion on aluminum nitride chip,” Submitted (2016).
- [38] A. Yamada and H. Shimizu, “Accurate analysis of $\delta v/v$ surface acoustic waveguides on a piezoelectric anisotropic substrate,” *Electron. Comm. Jpn* **1** **70**, 38 (1987).
- [39] C.-L. Zou, X. Han, L. Jiang, and H. X. Tang, “Acoustic mode trapping,” In preparation (2016).
- [40] C. Wang, B. Lichtenwalter, A. Friebel, and H. X. Tang, “A closed-cycle 1K refrigeration cryostat,” *Cryogenics* **64**, 5 (2014).
- [41] M. Aspelmeyer, T. J. Kippenberg, and F. Marquardt, “Cavity optomechanics,” *Rev. Mod. Phys.* **86**, 1391 (2014).
- [42] D. E. Chang, K.-K. Ni, O. Painter, and H. J. Kimble, “Ultrahigh-Q mechanical oscillators through optical trapping,” *New J. Phys.* **14**, 045002 (2012).
- [43] A. Noguchi, R. Yamazaki, M. Ataka, H. Fujita, Y. Tabuchi, T. Ishikawa, K. Usami, and Y. Nakamura, “Strong coupling in multimode quantum electromechanics,” *arXiv: 1602.01554* (2016).
- [44] J. Gao, *The physics of superconducting microwave resonators*, Ph.D. thesis, California Institute of Technology (2008).
- [45] C. A. Swenson, “Recommended Values for the Thermal Expansivity of Silicon from 0 to 1000 K,” *J. Phys. Chem. Ref. Data* **12**, 179 (1983).